Improving the Accuracy of Human Body Orientation Estimation With Wearable IMU Sensors

Hamad Ahmed, *Member, IEEE*, and Muhammad Tahir, *Member, IEEE*

***Abstract*— Accurately estimating the orientation of different human body segments using low cost inertial sensors is a key component in various activity-related and healthcare-related applications. Typically, the signals from a gyroscope and an accelerometer are fused inside a Kalman filter to determine the orientation. However, the accelerometer measurements are influenced by the linear accelerations of the body segments in addition to the gravitational acceleration that corrupts the orientation estimates. The conventional method to deal with linear acceleration is to model it as a first-order low-pass process and estimate it inside the Kalman filter. In this conventional method, important information from those sensor axes that do not experience linear accelerations is lost. In this paper, we modify the conventional approach to deal with the problem of linear acceleration more efficiently. The proposed approach estimates the direction of linear acceleration and assigns lower weights inside the Kalman filter to only those sensor axes that are experiencing acceleration, thus conserving important information from other axes measurements. The proposed method is compared with the conventional method using simulations and experimentation on a test subject performing daily routine tasks. The results indicate a significant performance improvement in orientation estimation.**

***Index Terms*— Human body orientation, Kalman filter, linear acceleration, wearable sensors.**

I. Introduction

ESTIMATING the orientation of the human body or a particular segment of it is central to various activity-related and healthcare-related applications [1], [2]. These include fall detection for safety of elderly people [3], [4], movement and analysis of body motion and postural orientation [5], [6], patient rehabilitation exercises [7], [8], exoskeletons for rehabilitation [9], [10], sports person's and athlete's limb dynamics [11], [12], and interactive gaming [13]. Wearable inertial measurement unit (IMU) sensors are also used in robotic prosthetic body parts, e.g., robotic arms or hands for determining orientation to provide stability and control [14], [15]. Traditional methods for determining the orientation were based on a simple camera [16], or more recently the 3-D camera called KINECT [17]. However, camera-based methods require hefty image processing and dedicated computers to run the image processing algorithms. Furthermore, bad lighting conditions and limited field of view are other limitations in using camera-based sensors.

Advances in MEMS technology have enabled tiny and low cost inertial sensors called IMU to be deployed in the orientation estimation of human body as wearable sensors. These are small in size and do not require hefty signal processing. An IMU consists of a triaxial gyroscope and a triaxial accelerometer. A gyroscope measures the angular rate of rotation about its axes and integrating these rates with respect to time yields the orientation angles; however, the integration process also accumulates any bias or sensor error and the orientation estimate begins to drift away after some time from the true orientation. An accelerometer determines the orientation by sensing the gravitational acceleration about its axes. This estimate is very noisy but does not drift because no integration is involved. Typically, the gyroscope measurements are fused with the accelerometer measurements through a Kalman filter in order to overcome the shortcomings of both the sensors and provide an accurate and acceptable orientation estimate.

One problem while using the accelerometer in sensor fusion is that if the body segment also moves linearly in addition to changing its orientation, the accelerometer measures linear accelerations as well in addition to the gravitational acceleration. The presence of these linear accelerations corrupts the orientation estimate during fusion [18]. Thus, the linear/external acceleration has to be dealt with carefully before fusing the accelerometer measurements with the gyroscope measurements. Three classical approaches exist in the literature to address the external acceleration problem. The first approach is the accelerometer norm-based thresholding approach [19], which makes use of the fact that a static accelerometer only measures gravitational acceleration, the norm of which is 9.8 m/s^2. If the norm of accelerometer measurements exceeds 9.8 m/s^2 by some threshold, then it must be experiencing external accelerations and is termed as being in a dynamic state. The estimation is then switched to gyroscope only until the dynamic state lasts. The problem with this approach is incorrect state detection, i.e., fluctuation due to sensor noise can cause incorrect state detection, and inability to deal with prolonged dynamic conditions because the estimation from only gyroscope will begin to drift after some time.

The second approach is the adaptive filtering approach [20], which makes use of the fact that the Kalman filter residual will be large if external accelerations are present since the orientation estimate from gyroscope and accelerometer will

Manuscript received August 13, 2016; accepted October 1, 2016. The Associate Editor coordinating the review process was Dr. Jesús Ureña.

The authors are with the Department of Electrical Engineering, Syed Babar Ali School of Science and Engineering, Lahore University of Management Sciences, Lahore 54792, Pakistan (e-mail: hamad.ahmed@lums.edu.pk; tahir@lums.edu.pk).

Color versions of one or more of the figures in this paper are available online at http://ieeexplore.ieee.org.

Digital Object Identifier 10.1109/TIM.2016.2642658

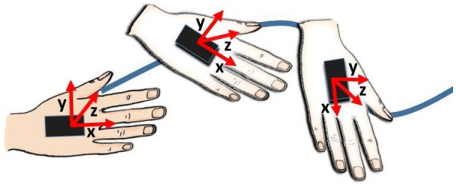

(a) Movement of hand

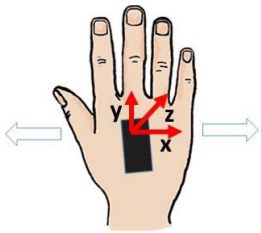

(b) Movement of hand

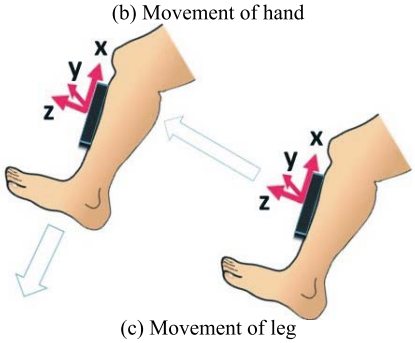

(c) Movement of leg

Fig. 1. Movements along single axis.

differ greatly. Hence, the weight of the accelerometer in the Kalman filter is scaled down according to the residual, which decreases the effect of external acceleration on the filter output. This approach is free from estimating the state of the sensor; however, for prolonged dynamic conditions, the estimate from this approach also begins to drift away as the estimation relies solely on gyroscope.

The third method is to model the external acceleration as a first-order stochastic process in order to estimate and successively remove it from the orientation estimate rather than switching the estimation to gyroscope only [21]. The first-order process model was shown to be adequate for estimating external accelerations of mild magnitudes. This method is superior to both the previous methods as it considers the estimation of external acceleration and never switches the estimation to gyroscope only. Further, the authors claim that the tuning of the parameters involved in the filter is easier compared to the previous methods. However, the proposed Kalman filter was not efficient in handling the weight of the accelerometer measurements in the filter when external accelerations were present. It assigned lower weights to all the accelerometer measurements even if a single axis experienced linear acceleration. From here on, we refer to this method as the conventional method.

We have observed that during most kinds of human motions, the movement is unlikely to be along more than one axis. This is demonstrated in Fig. 1(a) where the hand is moved randomly, however, the motion is always parallel to the z-axis of the instrumentation device, inducing accelerations in only z-axis. Similar is the case in Fig. 1(b), where the hand is waved and the accelerations are only along the x-axis. The scenario for walking is shown in Fig. 1(c), where the accelerations are first along the z-axis and then the x-axis. If we are able to separate out such axes of the instrumentation device, i.e., those axes that are undergoing linear acceleration then we can decrease the weight of only these axes, thus reserving important information from other axes. In this way, we can improve the performance of orientation estimation of human body segments.

In this paper, we propose a new measurement model for the Kalman filter, which estimates the direction of linear acceleration and then assigns lower weights to the corresponding accelerometer axes only by increasing their measurement noise covariance in the Kalman filter, thus preserving important information from other axes. In this way, we show that the estimation accuracy is improved significantly. It is important to note that the above-mentioned scenarios [Fig. 1(a)–(c)] only serve as a motivation for this paper. In the cases when the accelerations are along more than one axis, the proposed algorithm also performs better than the conventional one as demonstrated in the simulation and experiments. The proposed method achieves subdegree level of accuracy in certain scenarios, which the conventional method is not able to achieve in any scenario. We have used the Euler angle formulation of the Kalman filter to illustrate our concept, but it can also be applied to quaternions by transforming the corresponding equations to the quaternion domain. We are only concerned with pitch and roll orientation estimation and not the yaw estimation, because it uses a magnetometer instead of an accelerometer.

The rest of the paper is organized as follows. Section II describes the overall methodology, including the models used for sensors, process, and measurement models along with the details of the Kalman filter used for sensor fusion. Section III describes the working environment for the simulations setup where different types of scenarios have been simulated for comparing the proposed approach with the conventional one. Section IV describes the experimental setup and compares both the approaches in a number of cases involving different human body segment motions. Based on the discussion carried out in these sections, some conclusions are derived in Section V.

II. Methodology

A. Sensor Models

The measurements from the triaxial gyroscope and the triaxial accelerometer at time instant t are modeled as

$$\mathbf{y}_{G_t} = \boldsymbol{\omega}_t + \mathbf{n}_G \tag{1}$$

$$\mathbf{y}_{A_t} = \mathbf{g}_t + \mathbf{a}_t + \mathbf{n}_A \tag{2}$$

where in (1), $\mathbf{y}_{G_t}$ is a vector containing the gyroscope measurements, $\boldsymbol{\omega}_t$ contains the true angular rates about each gyroscope axis, and $\mathbf{n}_G$ contains the zero mean white Gaussian noise in these measurements. In (2), $\mathbf{y}_{A_t}$ contains the accelerometer measurements, $\mathbf{g}_t$ and $\mathbf{a}_t$ contain the gravitational accelerations and external accelerations about each accelerometer axis,

respectively, whereas $\mathbf{n}_A$ contains the white Gaussian noise in these accelerometer measurements.

B. External Acceleration Model

To model the external accelerations, we use a first-order process with the general form

$$a_t = c_a a_{t-1} + \varepsilon_t \tag{3}$$

where c_a is a dimensionless constant between 0 and 1, which gives the cutoff frequency and ε_t is the time-varying error of this model. We model the external acceleration along each of the three axes using this model, hence

$$a_{x_t} = c_a a_{x_{t-1}} + \varepsilon_{x_t} \tag{4}$$

$$a_{y_t} = c_a a_{y_{t-1}} + \varepsilon_{y_t} \tag{5}$$

$$a_{z_t} = c_a a_{z_{t-1}} + \varepsilon_{z_t} \tag{6}$$

which put into vector form, gives us

$$\mathbf{a}_t = c_a \mathbf{a}_{t-1} + \boldsymbol{\varepsilon}_t. \tag{7}$$

If we ignore correlated acceleration scenarios, then the error of the model for any axis (ε_{x_t}, ε_{y_t} or ε_{z_t}) is independent of the error in the other axes, hence the covariance matrix of $\boldsymbol{\varepsilon}_t$ should be a diagonal matrix.

C. State Vector

Let us denote the pitch, roll, and heading of the body segment by θ, ϕ, and ψ, respectively. The relationship between the earth coordinate frame ${}^{E}\mathbf{X}$ and the body coordinate frame ${}^{B}\mathbf{X}$ can be expressed as

$${}^{E}\mathbf{X} = \mathbf{R}\,{}^{B}\mathbf{X} \tag{8}$$

where $\mathbf{R}$ is the rotation matrix to rotate any vector in the body coordinate frame (${}^{B}\mathbf{X}$) into the earth coordinate frame (${}^{E}\mathbf{X}$). This rotation matrix is given as

$$\mathbf{R} = \begin{bmatrix} c\psi c\theta & c\psi s\theta s\phi - s\psi c\phi & c\psi s\theta c\phi + s\psi s\phi \\ s\psi c\theta & s\psi s\theta s\phi + c\psi c\phi & s\psi s\theta c\phi - c\psi s\phi \\ -s\theta & c\theta s\phi & c\theta c\phi \end{bmatrix} \tag{9}$$

where c and s denote the cos and sin operations. We observe that only the last row of the rotation matrix is sufficient to compute the pitch and roll angles as

$$\phi = \operatorname{atan}\left(\frac{R_{32}}{R_{33}}\right), \quad \theta = \operatorname{atan}\left(\frac{-R_{31}}{R_{32}/\sin\phi}\right). \tag{10}$$

So we define the state vector $\mathbf{x}$ at time t as

$$\mathbf{x}_t = \begin{bmatrix} R_{31} \\ R_{32} \\ R_{33} \end{bmatrix}. \tag{11}$$

Also note that in (2), the gravitational acceleration vector $\mathbf{g}_t$ at time t, measured in the body coordinate frame is given as

$$\mathbf{g}_t = g\mathbf{x}_t \tag{12}$$

where g is the gravitational acceleration constant 9.81 m/s^2. The general process and measurement models of the Kalman filter are given as

$$\mathbf{x}_t = \boldsymbol{\Phi}_{t-1}\mathbf{x}_{t-1} + \mathbf{w}_{t-1} \tag{13}$$

$$\mathbf{z}_t = \mathbf{H}\mathbf{x}_t + \mathbf{v}_t \tag{14}$$

where $\boldsymbol{\Phi}_{t-1}$ is the state transition matrix, $\mathbf{w}_{t-1} \sim \mathcal{N}(0, \mathbf{Q}_{t-1})$ where $\mathbf{Q}_{t-1}$ is the process noise covariance matrix, $\mathbf{z}_t$ is the measurement vector, $\mathbf{H}$ is the observation matrix, and $\mathbf{v}_t \sim \mathcal{N}(0, \mathbf{M}_t)$ where $\mathbf{M}_t$ is the measurement noise covariance matrix.

D. Process Model

The gyroscope measurements are used for propagating the state vector in the process model. We make use of the fact that the rotation matrix at time t, i.e., $\mathbf{R}_t$, can be computed from the rotation matrix at previous time instant $t-1$ using the integral of the vector differential equation as given in [22]

$$\mathbf{R}_t = \mathbf{R}_{t-1}(\boldsymbol{I}_3 + \Delta t\tilde{\boldsymbol{\omega}}_{t-1}) \tag{15}$$

where I_3 is a 3×3 identity matrix, Δt is the sampling time interval, and $\sim$ is an operator on any 3×1 vector $\mathbf{p} = [p1 \;\; p2 \;\; p3]^T$, which gives its skew-symmetric cross product [22]

$$\tilde{\mathbf{p}} = \begin{bmatrix} 0 & -p_3 & p_2 \\ p_3 & 0 & -p_1 \\ -p_2 & p_1 & 0 \end{bmatrix}. \tag{16}$$

Since we are only interested in the third row of $\mathbf{R}_t$ which is the state vector, hence instead of using (15) we can directly use

$$\mathbf{x}_t = (\boldsymbol{I}_3 + \Delta t\tilde{\boldsymbol{\omega}}_{t-1})\mathbf{x}_{t-1}. \tag{17}$$

Inserting (1) into (17), we obtain

$$\begin{aligned} \mathbf{x}_t &= (\boldsymbol{I}_3 + \Delta t\tilde{\mathbf{y}}_{G_{t-1}} - \Delta t\tilde{\mathbf{n}}_G)\mathbf{x}_{t-1} \\ &= (\boldsymbol{I}_3 + \Delta t\tilde{\mathbf{y}}_{G_{t-1}})\mathbf{x}_{t-1} + \Delta t\tilde{\mathbf{x}}_{t-1}\mathbf{n}_G \end{aligned} \tag{18}$$

where the last equation is obtained using the identities $\widetilde{\mathbf{p}-\mathbf{q}} = \tilde{\mathbf{p}} - \tilde{\mathbf{q}}$ and $\tilde{\mathbf{a}}\mathbf{b} = -\tilde{\mathbf{b}}\mathbf{a}$. Comparing (18) with the process model in (13), we obtain the state transition matrix and a model for the process noise

$$\boldsymbol{\Phi}_{t-1} = \boldsymbol{I}_3 + \Delta t\tilde{\mathbf{y}}_{G_{t-1}} \tag{19}$$

$$\mathbf{w}_{t-1} = \Delta t\tilde{\mathbf{x}}_{t-1}\mathbf{n}_G. \tag{20}$$

The process noise covariance matrix $\mathbf{Q}_{t-1}$ is given as

$$\mathbf{Q}_{t-1} = E\big[\mathbf{w}_{t-1}\mathbf{w}_{t-1}^T\big]. \tag{21}$$

Using (20) along with the identity $\tilde{\mathbf{x}}_{t-1}^T = -\tilde{\mathbf{x}}_{t-1}$, we arrive at

$$\mathbf{Q}_{t-1} = -\Delta t^2\tilde{\mathbf{x}}_{t-1}\boldsymbol{\Sigma}_G\tilde{\mathbf{x}}_{t-1}. \tag{22}$$

Here $\boldsymbol{\Sigma}_G$ is the covariance matrix of gyroscope's measurement noise given by $E[\mathbf{n}_G\mathbf{n}_G^T]$ which is set equal to $\sigma_G^2\boldsymbol{I}_3$ by assuming that the variance of gyroscope measurement noise σ_G^2 is the same along all the three axes.

E. Measurement Model

The predicted acceleration $\mathbf{a}_t^{\text{pred}}$ is obtained from the estimated acceleration of previous time instant $\mathbf{a}_{t-1}^{\text{est}}$ according to the acceleration model in (7) as

$$\mathbf{a}_t^{\text{pred}} = c_a \cdot \mathbf{a}_{t-1}^{\text{est}}. \tag{23}$$

The error between this prediction and the true acceleration $\mathbf{a}_t$ is

$$\boldsymbol{\varepsilon}_t = \mathbf{a}_t - \mathbf{a}_t^{\text{pred}}. \tag{24}$$

Inserting (23) and (24) into (2)

$$\mathbf{y}_{A_t} = g\mathbf{x}_t + c_a\mathbf{a}_t^{\text{pred}} + \boldsymbol{\varepsilon}_t + \mathbf{n}_A \tag{25}$$

$$\mathbf{y}_{A_t} = g\mathbf{x}_t + c_a\mathbf{a}_{t-1}^{\text{est}} + \boldsymbol{\varepsilon}_t + \mathbf{n}_A \tag{26}$$

$$\mathbf{y}_{A_t} - c_a\mathbf{a}_{t-1}^{\text{est}} = g\mathbf{x}_t + \boldsymbol{\varepsilon}_t + \mathbf{n}_A. \tag{27}$$

Comparing (27) with (14) we obtain the measurement vector $\mathbf{z}_t$, observation matrix $\mathbf{H}$, and a model for the measurement noise $\mathbf{v}_t$

$$\mathbf{z}_t = \mathbf{y}_{A_t} - c_a \cdot \mathbf{a}_{t-1}^{\text{est}} \tag{28}$$

$$\mathbf{H} = g\mathbf{I}_3 \tag{29}$$

$$\mathbf{v}_t = \boldsymbol{\varepsilon}_t + \mathbf{n}_A. \tag{30}$$

Since $\boldsymbol{\varepsilon}_t$ and $\mathbf{n}_A$ are uncorrelated, we can write the measurement noise covariance $\mathbf{M}_t$ as

$$\mathbf{M}_t = E\left[\mathbf{v}_{t-1}\mathbf{v}_{t-1}^T\right] = \boldsymbol{\Sigma}_{a_t} + \boldsymbol{\Sigma}_A. \tag{31}$$

$\boldsymbol{\Sigma}_A$ is set equal to $\sigma_A^2\boldsymbol{I}_3$ by assuming that the variance of accelerometer measurement noise σ_A^2 is the same along all of its axes. The expression for $\boldsymbol{\Sigma}_{a_t}$ can be written as [21]

$$\boldsymbol{\Sigma}_{a_t} = c_a^2 E\left[\mathbf{a}_{t-1}^{\text{est}}\mathbf{a}_{t-1}^{\text{est}\ T}\right]. \tag{32}$$

Since (32) cannot be solved analytically, the method in [21] (the conventional method) distributes the vector norm of $\mathbf{a}_{t-1}^{\text{est}}$ along the diagonals of $\boldsymbol{\Sigma}_{a_t}$ to obtain the following expression:

$$\boldsymbol{\Sigma}_{a_t} = 3^{-1}c_a^2\left|\left|\mathbf{a}_{t-1}^{\text{est}}\right|\right|^2\mathbf{I}_3. \tag{33}$$

As a result of using (33), the noise covariance of all the three accelerometer measurements are equally weighted in all the scenarios of external acceleration. This is not an efficient approach especially for those cases where only a single axis of accelerometer experiences linear acceleration such as the case of wearable sensors estimating human body orientation. In addition, if more than one axis of the accelerometer experience linear accelerations, an efficient approach would be to weigh each axis according to the severity of acceleration. Motivated by this idea, we approximate the expectation operator in (32) by taking the mean over a fixed window of size M_1 and set $\boldsymbol{\Sigma}_{a_t}$ as

$$\boldsymbol{\Sigma}_{a_t} = \frac{1}{M_1}c_a^2\sum_{i=1}^{M_1}\mathbf{a}_{t-i}^{\text{est}}\mathbf{a}_{t-i}^{\text{est}^T}. \tag{34}$$

In this way, the covariance of only that axis is increased which experiences acceleration. In the case that more than one axis experiences linear acceleration, their respective variances are automatically increased in proportion to the severity of the acceleration present on that axis. M_1 is the length of the window over which the averaging operation is performed to approximate the expectation operator. A larger window will average accelerations over a longer history in time and introduce a certain lag in the filter, whereas a very short window will not perform well in high speed dynamics, compromising the performance of the filter. A particular example of this case is when the accelerometer measurements switch from positive to negative, exhibiting a zero crossing. Therefore, the value should be set by tuning to get the desired performance.

The $\boldsymbol{\Sigma}_{a_t}$ formed according to our method by (34) does not yield a diagonal matrix, whereas we remarked in Section II-B that it should be a diagonal matrix. As the acceleration model error for any axis is independent of the acceleration model error of the other axes, we diagonalize $\boldsymbol{\Sigma}_{a_t}$ by retaining only its diagonal entries

$$\boldsymbol{\Sigma}_{a_t} = \frac{1}{M_1}c_a^2 \cdot \text{diag}\left(\sum_{i=1}^{M_1}\mathbf{a}_{t-i}^{\text{est}}\mathbf{a}_{t-i}^{\text{est}^T}\right). \tag{35}$$

Note that this step is not necessary and can be omitted if the reader chooses not to make the assumption of independent accelerations and further suppress the errors due to correlated accelerations in the filter as the nondiagonal, nonzero elements signify the measurement covariance of different accelerometer axes measurements.

F. Filter Procedure

Once the process and noise models have been defined, the general procedure of the Kalman filter is as follows:

$$\mathbf{x}_t^- = \boldsymbol{\Phi}_{t-1}\mathbf{x}_{t-1}^+ \tag{36}$$

$$\mathbf{P}_t^- = \boldsymbol{\Phi}_{t-1}\mathbf{P}_{t-1}^+\boldsymbol{\Phi}_{t-1}^T + \mathbf{Q}_{t-1} \tag{37}$$

$$\mathbf{K}_t = \mathbf{P}_t^-\mathbf{H}^T\left(\mathbf{H}\mathbf{P}_t^-\mathbf{H}^T + \mathbf{M}_t\right)^{-1} \tag{38}$$

$$\mathbf{x}_t^+ = \mathbf{x}_t^- + \mathbf{K}_t\left(\mathbf{z}_t - \mathbf{H}\mathbf{x}_t^-\right) \tag{39}$$

$$\mathbf{P}_t^+ = (\mathbf{I} - \mathbf{K}_t\mathbf{H})\mathbf{P}_t^- \tag{40}$$

where superscript $-$ denotes *a priori* and superscript $+$ denotes *a posteriori* state estimate. We can calculate the pitch & roll angle from the *a posteriori* state estimate

$$\phi_t = \text{atan}\left(\frac{\mathbf{x}_t^+(1)}{\mathbf{x}_t^+(2)}\right) \quad \theta_t = \text{atan}\left(\frac{-\mathbf{x}_t^+(1)}{\mathbf{x}_t^+(2)/\sin\phi_t}\right) \tag{41}$$

and the external acceleration can be estimated as

$$\mathbf{a}_t^{\text{est}} = \mathbf{y}_{A_t} - g\mathbf{x}_t^+. \tag{42}$$

G. Analysis and Discussion

In this section, we theoretically analyze and establish how the proposed approach will perform better than the conventional one. The purpose of the measurement update inside the Kalman filter is to mitigate the error propagated in the state estimate from the process model. Let the *a priori* estimate $\mathbf{x}_t^-$ be given as

$$\mathbf{x}_t^- = \mathbf{x}_t + \delta\mathbf{x}_t \tag{43}$$

where $\delta\mathbf{x}_t$ is the error in the *a priori* estimate and $\mathbf{x}_t$ is the true state. The *a posteriori* estimate obtained after measurement update is given by (39). Inserting (43) and (14) into (39), we obtain

$$\mathbf{x}_t^+ = (\mathbf{x}_t + \delta\mathbf{x}_t) + \mathbf{K}_t(\mathbf{H}\mathbf{x}_t + \mathbf{v}_t - \mathbf{H}\mathbf{x}_t - \mathbf{H}\delta\mathbf{x}_t) \tag{44}$$

$$= \mathbf{x}_t + (\mathbf{I} - \mathbf{K}_t\mathbf{H})\delta\mathbf{x}_t + \mathbf{K}_t\mathbf{v}_t. \tag{45}$$

Comparing (45) with (43), we observe that the error $\delta\mathbf{x}_t$ propagated in the state estimate by the process model has been

reduced by the factor $(\mathbf{I}-\mathbf{K}_t\mathbf{H})$ in the *a posteriori* estimate. The amount of reduction depends upon the Kalman gain $\mathbf{K}_t$ computed in (38). Inserting (31) into (38), we obtain

$$\mathbf{K}_t = \mathbf{P}_t^- \mathbf{H}^T (\mathbf{H}\mathbf{P}_t^- \mathbf{H}^T + \mathbf{\Sigma}_A + \mathbf{\Sigma}_{a_t})^{-1}. \tag{46}$$

For the sake of simplicity, here we assume that $\mathbf{P}_t^- = P\mathbf{I}_3$. Note that this assumption has been made only in this section to simplify the analysis. Otherwise, in actual simulations and in the experimental results presented in the following section, we have not made any such assumption. Since $\mathbf{H} = g\mathbf{I}_3$, the Kalman gain formed using the method in [21] will be

$$\mathbf{K}_t = gP\mathbf{I}_3\big[g^2P\mathbf{I}_3 + \sigma_A^2\mathbf{I}_3 + 3^{-1}c_a^2||\mathbf{a}_{t-1}^{\text{est}}||^2\mathbf{I}_3\big]^{-1} \tag{47}$$

$$= \frac{gP}{g^2P + \sigma_A^2 + 3^{-1}c_a^2||\mathbf{a}_{t-1}^{\text{est}}||^2}\mathbf{I}_3 \tag{48}$$

$$= \frac{gP}{C_1 + 3^{-1}c_a^2||\mathbf{a}_{t-1}^{\text{est}}||^2}\mathbf{I}_3 \tag{49}$$

where $C_1 = g^2P + \sigma_A^2$. We can see that the Kalman gain computed by this method is the same for all the three axes. The Kalman gain formed by the proposed approach will be

$$\mathbf{K}_t = gP\mathbf{I}_3\big[g^2P\mathbf{I}_3 + \sigma_A^2\mathbf{I}_3 + \mathbf{\Sigma}_{a_t}\big]^{-1}. \tag{50}$$

For $M_1 = 1$, the covariance matrix $\mathbf{\Sigma}_{a_t}$ is given by

$$\mathbf{\Sigma}_{a_t} = c_a^2.\text{diag}\big(\mathbf{a}_{t-i}^{\text{est}}\mathbf{a}_{t-i}^{\text{est}^T}\big) \tag{51}$$

$$= c_a^2\begin{bmatrix} a_{x_{t-1}}^2 & & \\ & a_{y_{t-1}}^2 & \\ & & a_{z_{t-1}}^2 \end{bmatrix}. \tag{52}$$

Substituting the above expression for $\mathbf{\Sigma}_{a_t}$ into (50), we obtain

$$\mathbf{K}_t = gP\mathbf{I}_3\left[g^2P\mathbf{I}_3 + \sigma_A^2\mathbf{I}_3 + c_a^2\begin{bmatrix} a_{x_{t-1}}^2 & & \\ & a_{y_{t-1}}^2 & \\ & & a_{z_{t-1}}^2 \end{bmatrix}\right]^{-1}$$

$$= \begin{bmatrix} \frac{gP}{C_1 + c_a^2a_{x_{t-1}}^2} & & \\ & \frac{gP}{C_1 + c_a^2a_{y_{t-1}}^2} & \\ & & \frac{gP}{C_1 + c_a^2a_{z_{t-1}}^2} \end{bmatrix}. \tag{53}$$

Comparing (53) with (49) and noting the fact that

$$||\mathbf{a}_{t-1}||^2 = a_{x_{t-1}}^2 + a_{y_{t-1}}^2 + a_{z_{t-1}}^2 \tag{54}$$

we can observe that if the device experiences acceleration along any single axis (say x-axis), the conventional method reduces the gain of all the three axes equally, which decreases the correction of error in the *a priori* state estimate of the remaining two axes as well. The proposed method however, decreases the gain of only the x-axis according to (53) and allows correction of error in the remaining two axes.

Similar will be the case for the acceleration present along two axes. Even if the sensor is experiencing accelerations along all the three axes, the conventional method will equally reduce the gain for all the three axes causing the maximum of the three accelerations to affect the three axes. The proposed method, however, decreases each axis's gain according to the severity of the acceleration present in that axis. In this way, the proposed approach handles the external accelerations in a more efficient way. It can be seen from (54) that the maximum error incurred by the proposed approach cannot be more than that in the conventional approach.

TABLE I

ACCELERATIONS ADDED IN TESTS (m/s^2)

	Test 1			Test 2			Test 3		
	a_x	a_y	a_z	a_x	a_y	a_z	a_x	a_y	a_z
Mean	0	0	3.19	0	0.41	7.6	0.23	0.25	0
Max.	0	0	15.8	0	1.14	16.4	0.49	0.79	0

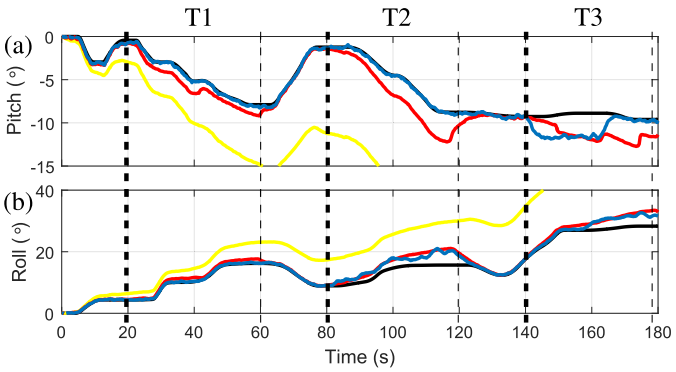

Fig. 2. (a) Pitch estimation results. (b) Roll estimation results. Black curve: reference. Yellow curve: gyro-based estimate. Red curve: conventional method. Blue curve: proposed method. Thick dashed line indicates start of test and thin dashed line indicates end of test.

TABLE II

RMS SIMULATED ATTITUDE ESTIMATION ERROR IN (°)

	Test 1		Test 2		Test 3	
	Pitch	Roll	Pitch	Roll	Pitch	Roll
Conventional Method	1.04	1.00	2.18	3.12	2.30	2.90
Proposed Method	**0.16**	**0.15**	**0.12**	**2.80**	**1.91**	**2.40**

III. SIMULATION RESULTS

To confirm and verify the expected performance gain of the proposed filter, an IMU sensor was simulated in MATLAB SIMULINK. Simulations were performed as they provide the freedom to selectively test the algorithm for accelerations of different durations along different axes. Both the methods were implemented to compare the results under the events when linear movement was being performed in addition to the change in the orientation of the body part.

Three different tests were performed. Fig. 2(a) and (b) shows the estimation results using three methods: using only gyroscope, the conventional method, and the proposed method for the three tests. The accelerations added in these tests are summarized in Table I, while the root-mean-square (RMS) error in estimation is provided in Table II.

In the first test, the accelerations are added in the z-axis during the time interval 20–60 s. c_a was set to 0.1 as recommended in [21]. The gyroscope-based estimate drifts with time, as expected. The conventional approach senses

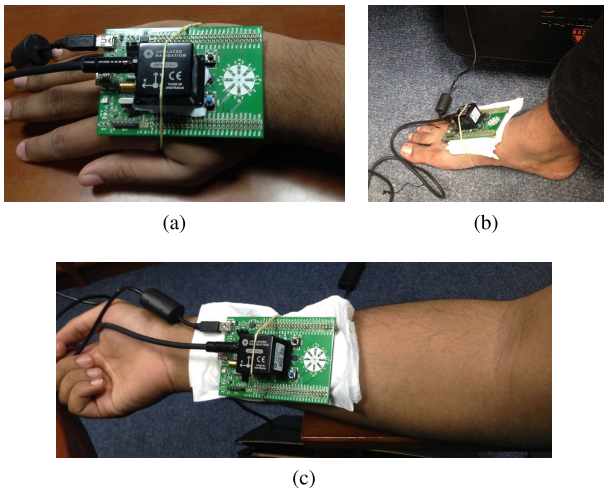

Fig. 3. IMU device (green) and reference measurement unit (black) installed on hand, foot, and arm of test subject.

linear acceleration and discards all three accelerometer measurements, losing information from x- and y- axes as well, hence both pitch and roll drift away, whereas the proposed method only discards z-axis measurements, preserving the accuracy in pitch and roll estimates.

Test 2 was performed during 80–120 s where the accelerations were added in the y and z-axes. Since the roll estimate depends upon the y-axis and both the methods observe error in roll estimate, the conventional approach also incurs error in pitch estimate, whereas the proposed filter maintains accurate pitch estimate. Note that the duration of the test is the same as Test 1, however, the conventional method observes more error in the pitch estimate than it does in Test 1. This is because two axes experience accelerations in test 2 which makes the total magnitude of accelerations larger compared to Test 1. This further decreases the weight of the accelerometer according to the conventional method, causing more error.

In Test 3, the acceleration is added in x-axis from 140–165 s and in y-axis from 155 to 180 s. The conventional method senses continuous accelerations during the whole time interval of 140–180 s and the estimate continues to drift. However, the proposed method quickly determines which axis is experiencing acceleration and only the respective estimate drifts during that time period.

IV. Experimental Results

To verify the accuracy of the proposed approach in estimating the orientation of human body segments, experiments were performed on a test subject equipped with wearable IMU sensors and an expensive accurate sensor that is not affected by external accelerations for reference measurements (Fig. 3). STMicroelectronics F3 discovery board was used as the wearable IMU sensor containing triaxial gyroscope (L3GD20) and triaxial accelerometer (LSM303DHLC) and a tactical grade IMU from Advanced Navigation Technologies with a maximum orientation estimation error of 0.1° was used as the reference measurement unit. Three different experiments were performed, where the subject was asked to perform the following tasks: hand wave, exercising, and walking. The value

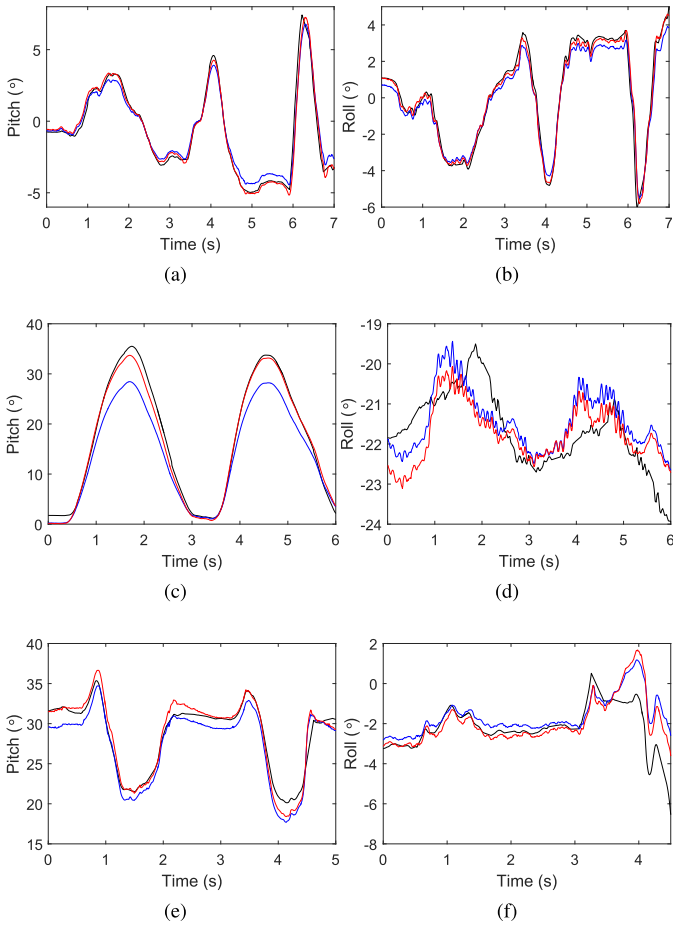

Fig. 4. Experimental results of pitch and roll estimation. -Black curve: reference. Blue curve: conventional method. Red curve: proposed method. (a) Pitch estimation of hand wave experiment. (b) Roll estimation of hand wave experiment. (c) Pitch estimation of arm experiment. (d) Roll estimation of arm experiment. (e) Pitch estimation of walking experiment. (f) Roll estimation of walking experiment.

of c_a was 0.1 and the length of M_1 was 15 for the algorithms. The test results are numerically presented in Table III.

For the first experiment, the IMU was installed on the hand for the first experiment, i.e., the hand wave test. The estimation results are shown in Fig. 4(a) and (d). This test included mild accelerations as it is difficult to induce high accelerations in hand motions. Both the methods perform almost the same in the roll estimation, however, in pitch estimation, the proposed method performs better than the conventional method. The difference can be observed specifically between 1.5 s and 5 s.

The second experiment was exercising, in which the IMU was installed on the arm of the subject that lifted a dumbbell as a bicep exercise. The estimation results are shown in Fig. 4(c) and (d). This test induced accelerations in the z-axis of the device. The pitch response is over a large range, hence differences are not visible from the plot but the differences in the roll estimation are visible in Fig. 4(d), where the proposed method achieves better accuracy than the conventional method.

The estimation results for the walking test are shown in Fig. 4(e) and (f). This test induced large accelerations along all axes but mostly in the z- and y-axes. The proposed method outperforms the conventional one in both pitch and roll

TABLE III
RMS EXPERIMENTAL ATTITUDE ESTIMATION ERROR (°)

	Hand Exp.		Arm Exp.		Walking Exp.	
	Pitch	Roll	Pitch	Roll	Pitch	Roll
Conventional Method	0.95	1.10	3.53	1.53	1.33	0.93
Proposed Method	**0.48**	**0.52**	**1.63**	**0.94**	**0.93**	**0.22**

TABLE IV
RMS ACCELERATION ESTIMATION ERROR IN (m/s^2)

	Hand Exp.			Arm Exp.			Walking Exp.		
	a_x	a_y	a_z	a_x	a_y	a_z	a_x	a_y	a_z
Conv. Method	0.58	0.51	0.83	3.04	2.45	1.20	1.57	1.20	2.60
Prop. Method	**0.41**	**049**	**0.79**	**0.89**	**0.94**	**0.99**	**1.34**	**0.94**	**1.40**

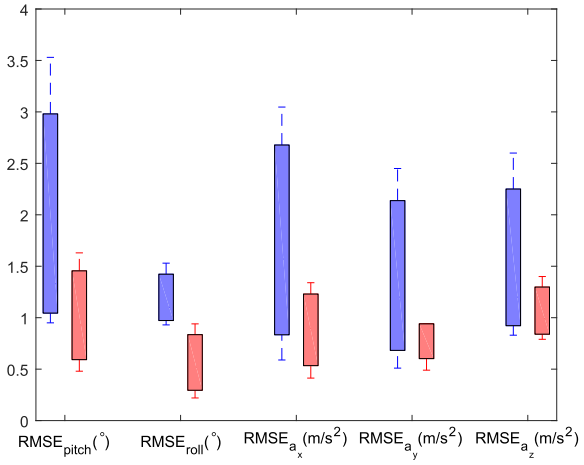

Fig. 5. Boxplot comparison of RMS error in pitch, roll, and external acceleration estimation along all three axes for the conventional and proposed approach.

response. Accelerations in the three axes corrupt the attitude estimate, however, the proposed method still performs much better than the conventional method in both pitch and roll estimates.

Each of the three experiments were then repeated ten times. Table III summarizes RMS attitude estimation error performance of both the methods in these experiments. The estimation results indicate that the proposed method always performs better than the conventional method in all the experiments. This is achieved due to better handling of linear accelerations inside the measurement model of the proposed method. Even if all the axes experience accelerations, they are better managed in the proposed method leading to better accuracy.

The true external acceleration was also obtained from the reference measurement unit by subtracting gravitational acceleration from its accelerometer's measurements according to (2) and (12) and the error in external acceleration estimation for both the approaches was computed, which is presented in Table IV. It can be seen that the acceleration estimation accuracy of the proposed approach is higher than the

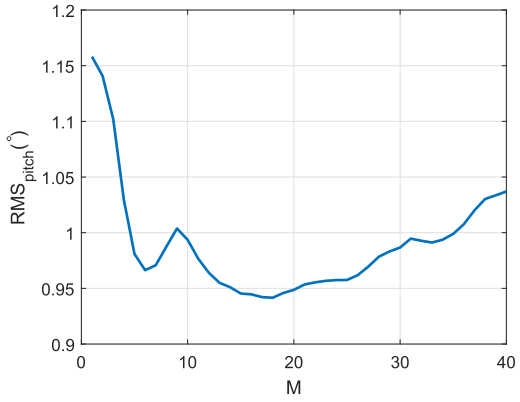

Fig. 6. Attitude Error as a function of Window Size M.

conventional method, which leads to higher accuracy of attitude estimation.

Fig. 5 shows the boxplot comparison of the proposed approach with the conventional approach for pitch, roll, and external acceleration estimation errors. It is easy to infer that the proposed approach introduces a useful level of improvement over the conventional approach.

As remarked in Section II-E, the value of M_1 should be set to a medium value such that the filter should neither lag, nor be too fast. To experimentally test the algorithm for various values of M_1, the pitch estimation for walking experiment was done for various values of M_1 and the estimation error against M_1 values is plotted in Fig. 6. It can be seen that the error is large for very small values but is optimum for a medium value of M_1. It begins to increase if the value keeps increasing because the filter starts to lag. Hence, the value should be tuned to get the desired performance.

V. CONCLUSION

Wearable IMU sensors have gained widespread usage in the orientation estimation of various human body segments owing to their miniature size and low cost. However, linear accelerations of the body segments remain a problem as they are also measured by the accelerometer, which corrupt the attitude estimate. The conventional method to deal with these accelerations does not effectively handle the accelerometer measurement weights in the Kalman filter and discards all three axis measurements if any axis experiences linear acceleration. In this paper, we proposed an important modification to this method. Using the fact that a majority of human body measurements are constrained in one or two axes and seldom in all three axes, the proposed method deals with the linear accelerations more effectively by discarding only those accelerometer measurements that are corrupted by acceleration, keeping useful information from other axes. A theoretical analysis has been carried out, which provides insight into the performance improvement obtained through the proposed method compared to the conventional one. Finally, both methods have been compared using simulations and experiments on a real test subject performing daily routine tasks like lifting and walking. The results show the performance improvement achieved in the case of the proposed method.

REFERENCES

[1] S. C. Mukhopadhyay, "Wearable sensors for human activity monitoring: A review," *IEEE Sensors J.*, vol. 15, no. 3, pp. 1321–1330, Mar. 2015.

[2] G. Ciuti, L. Ricotti, A. Menciassi, and P. Dario, "MEMS sensor technologies for human centred applications in healthcare, physical activities, safety and environmental sensing: A review on research activities in Italy," *Sensors*, vol. 15, no. 3, pp. 6441–6468, 2015.

[3] G. Shi, C. S. Chan, W. J. Li, K.-S. Leung, Y. Zou, and Y. Jin, "Mobile human airbag system for fall protection using MEMS sensors and embedded SVM classifier," *IEEE Sensors J.*, vol. 9, no. 5, pp. 495–503, May 2009.

[4] T. Shany, S. J. Redmond, M. R. Narayanan, and N. H. Lovell, "Sensors-based wearable systems for monitoring of human movement and falls," *IEEE Sensors J.*, vol. 12, no. 3, pp. 658–670, Mar. 2012.

[5] Y.-C. Kan and C.-K. Chen, "A wearable inertial sensor node for body motion analysis," *IEEE Sensors J.*, vol. 12, no. 3, pp. 651–657, Mar. 2012.

[6] L. T. D'Angelo, J. Neuhaeuser, Y. Zhao, and T. C. Lueth, "SIMPLE-use—Sensor set for wearable movement and interaction research," *IEEE Sensors J.*, vol. 14, no. 4, pp. 1207–1215, Apr. 2014.

[7] S. Patel, H. Park, P. Bonato, L. Chan, and M. Rodgers, "A review of wearable sensors and systems with application in rehabilitation," *J. Neuroeng. Rehabil.*, vol. 9, no. 1, p. 1, 2012.

[8] S. Mazilu *et al.*, "GaitAssist: A wearable assistant for gait training and rehabilitation in Parkinson's disease," in *Proc. IEEE Int. Conf. Pervasive Comput. Commun. Workshops (PERCOM Workshops)*, Mar. 2014, pp. 135–137.

[9] W.-W. Wang and L.-C. Fu, "Mirror therapy with an exoskeleton upper-limb robot based on IMU measurement system," in *Proc. IEEE Int. Workshop Med. Meas. Appl. (MeMeA)*, May 2011, pp. 370–375.

[10] C. Cifuentes, A. Braidot, L. Rodríguez, M. Frisoli, A. Santiago, and A. Frizera, "Development of a wearable ZigBee sensor system for upper limb rehabilitation robotics," in *Proc. 4th IEEE RAS EMBS Int. Conf. Biomed. Robot. Biomechatronics (BioRob)*, Jun. 2012, pp. 1989–1994.

[11] K. King, S. W. Yoon, N. C. Perkins, and K. Najafi, "Wireless MEMS inertial sensor system for golf swing dynamics," *Sens. Actuators A, Phys.*, vol. 141, no. 2, pp. 619–630, 2008.

[12] R. S. McGinnis and N. C. Perkins, "A highly miniaturized, wireless inertial measurement unit for characterizing the dynamics of pitched baseballs and softballs," *Sensors*, vol. 12, no. 9, pp. 11933–11945, 2012.

[13] S. Antifakos and B. Schiele, "Bridging the gap between virtual and physical games using wearable sensors," in *Proc. 6th Int. Symp. Wearable Comput. (ISWC)*, Oct. 2002, pp. 139–140.

[14] J. A. Corrales, F. A. Candelas, and F. Torres, "Hybrid tracking of human operators using IMU/UWB data fusion by a Kalman filter," in *Proc. 3rd ACM/IEEE Int. Conf. Human-Robot Interact. (HRI)*, Mar. 2008, pp. 193–200.

[15] M. El-Gohary and J. McNames, "Shoulder and elbow joint angle tracking with inertial sensors," *IEEE Trans. Biomed. Eng.*, vol. 59, no. 9, pp. 2635–2641, Sep. 2012.

[16] C. Plagemann, V. Ganapathi, D. Koller, and S. Thrun, "Real-time identification and localization of body parts from depth images," in *Proc. IEEE Int. Conf. Robot. Autom. (ICRA)*, May 2010, pp. 3108–3113.

[17] Z. Zhang, "Microsoft Kinect sensor and its effect," *IEEE MultiMedia*, vol. 19, no. 2, pp. 4–10, Feb. 2012.

[18] H. Ahmed and M. Tahir, "Terrain-based vehicle localization using low cost MEMS-IMU sensors," in *Proc. IEEE 83rd Veh. Technol. Conf. (VTC)*, May 2016, pp. 1–5.

[19] T. Harada, H. Uchino, T. Mori, and T. Sato, "Portable absolute orientation estimation device with wireless network under accelerated situation," in *Proc. IEEE Int. Conf. Robot. Autom. (ICRA)*, vol. 2. May 2004, pp. 1412–1417.

[20] Y. S. Suh, "Orientation estimation using a quaternion-based indirect Kalman filter with adaptive estimation of external acceleration," *IEEE Trans. Instrum. Meas.*, vol. 59, no. 12, pp. 3296–3305, Dec. 2010.

[21] J. K. Lee, E. J. Park, and S. N. Robinovitch, "Estimation of attitude and external acceleration using inertial sensor measurement during various dynamic conditions," *IEEE Trans. Instrum. Meas.*, vol. 61, no. 8, pp. 2262–2273, Aug. 2012.

[22] S. Ayub, A. Bahraminisaab, and B. Honary, "A sensor fusion method for smart phone orientation estimation," in *Proc. 13th Annu. Post Graduate Symp. Converg. Telecommun. Netw. Broadcast.*, Liverpool, U.K., 2012.

Hamad Ahmed (M'15) received the B.Sc. degree in electrical engineering with majors in telecommunication and electronics engineering from the University of Engineering and Technology, Lahore, Pakistan, in 2015.

He was a Research Assistant with the Signal Processing and Navigation Algorithms Group, Department of Electrical Engineering, Lahore University of Management Sciences, Lahore, where he was involved in the development of low cost alternatives to GPS for vehicle localization. His current research interests include statistical signal processing, optimal estimation theory, wireless localization techniques, and machine learning.

Muhammad Tahir (M'15) received the M.S. and Ph.D. degrees in electronics and communication engineering from the Politecnico di Torino, Turin, Italy, in 2009 and 2013, respectively.

In 2013, he joined the Navigation Signal Analysis and Simulation Group, Istituto Superiore Mario Boella, Turin, as a Research Associate. In 2014, he joined the Electrical Engineering Department, Lahore University of Management Sciences, Lahore, Pakistan, as an Assistant Professor. His current research interests include statistical signal processing, estimation and detection theory, and nonlinear Bayesian filtering with applications to wireless positioning, navigation, and communications.